

4.5 Meso-Scale Model (JMA-MSM0603)

4.5.1 Introduction

The Meso-scale numerical prediction system has been operational since March 2001 to provide additional information for disaster prevention and aviation safety. In the beginning, the Meso-Scale Model (MSM) was a hydrostatic spectral model which was also used as the Regional Spectral Model (RSM) in different configuration described in section 4.4. The horizontal resolution of the MSM was 10km and the 40 vertical layers were set. The MSM produced 18 hour forecast every 6 hours at 00, 06, 12, 18UTC.

In September 2004, the hydrostatic spectral model was replaced with a nonhydrostatic grid model. The new MSM employed full-compressible elastic equations including a map factor. The general configurations of the system like resolution, forecast time, forecast frequency and so on, were kept almost the same to those of the previous system.

The last major upgrade of the system was executed in March 2006 to enhance the disaster information and enrich the forecast for aviation safety. The horizontal resolution became higher from 10km to 5km to resolve the finer-scale weather phenomena. The forecast frequency was increased from 4 times to 8 times (00, 03, 06, 09, 12, 15, 18 and 21UTC initial time) to provide more accurate forecasts although the forecast time is shortened from 18 hours to 15 hours. Besides the improvement of the system configurations, most physical processes were also modified so that the missing ratio of intense rainfall was reduced significantly and the diurnal variation of near-surface variables was simulated better.

4.5.2 General Configurations

The MSM provides 15 hour forecast every 3 hours: 00, 03, 06, 09, 12, 15, 18, 21UTC. The forecast domain is the rectangular area of about 3600km x 2880km with the grid spacing of 5km (Fig. 4.5.1). The MSM employs the Lambert conformal conic map projection. In the vertical, the terrain following coordinate is adopted. The model top is set to 21,800m with 50 layers whose intervals vary linearly from 40m at bottom to 904m at top.

A forecast model of the MSM is the JMA nonhydrostatic model (Saito et al. 2006). The prognostic variables are horizontal and vertical momentum, potential temperature, pressure, mixing ratios of water vapor and hydrometeors (cloud water, cloud ice, rain, snow and graupel), the ground temperature and the wetness.

The meso-scale analysis by the Meso 4D-Var (see Sec.3.7) is used as the initial conditions. The vertical momentum

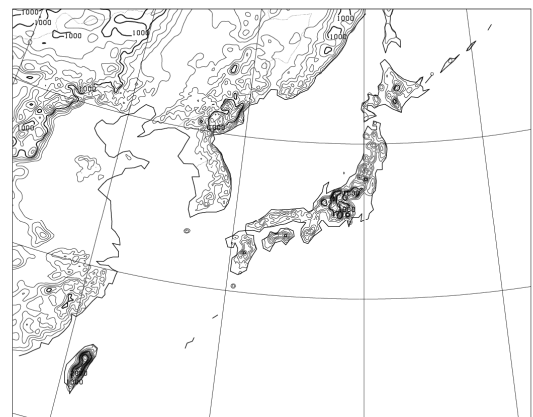


Fig. 4.5.1 Forecast domain and topography of the MSM. The contour interval is 100m.

and the pressure aloft are diagnosed to satisfy the continuity equation and the hydrostatic equation, respectively. Other microphysics variables except water vapor are carried on from the 3 hourly forecast of a previous run, these quantities are set to zero where the humidity of the analysis is less than 90%. As for the lateral boundary conditions, the MSM is nested in the RSM although hydrometeors are not provided by the RSM.

The data source of the model terrain is the GTOPO30 data set. The data is smoothed so that the valid resolution of the model terrain is about 7.5km. The land-sea distribution and the surface parameters such as the heat capacity, the thermal conductivity, albedo, initial wetness and roughness are determined based on the Global Land Cover Characteristics (GLCC) data set for land use. Both GTOPO30 and GLCC data sets are developed by U.S. Geological Survey's EROS Data Center.

Surface kinds are classified into 4 categories, land, sea, snow covered area and ice covered area, according to the analysis that is updated every 3 hours with grid spacing of 10km. Snow covered areas are analyzed by the snow depth data of the Global snow depth analysis (see Sec.3.9) and then, the areas within a 60km radius of observation sites of the domestic SYNOP and Automated Meteorological Data Acquisition System (AMeDAS) are modified by their snow depth data at the analysis time. If the snow depth is larger than 5cm, a corresponding grid is classified to be the snow covered area. Ice covered areas are identified from the sea ice analysis conducted by JMA. Over snow and ice covered areas, surface parameters previously determined based on GLCC data are modified with the predetermined values.

On land, snow covered area and ice covered area, the underground temperature is predicted by the 4-layer thermal diffusion model whose layers are numbered from the surface. The fields of the 1st and 2nd layers are initialized by the forecast of the MSM in the outer loop of the Meso 4D-Var and the fields of the 3rd and 4th layers are reset to climate data. At sea, the surface temperature is linearly interpolated from the SST analysis (see Sec.6.2). It is given as the underground temperature of the 1st layer and is kept constant.

4.5.3 Dynamics

a) Basic equations

The governing equations of MSM0603 consist of non-hydrostatic, fully compressible equations on a spherical curvilinear orthogonal and a terrain-following coordinate with shallow assumption. Details of the derivations of these equations are given in Saito et al. 2006.

(a-1) Flux form momentum equations

The equations of motion are described in the flux form:

$$\frac{\partial U}{\partial t} + \frac{m_1}{m_2} \left(\frac{\partial P}{\partial \hat{x}} + \frac{\partial G^{13} P}{\partial \hat{z}} \right) = -ADVU + RU, \quad (4.5.1)$$

$$ADVU = m_1 \left(\frac{\partial Uu}{\partial \hat{x}} + \frac{\partial Vu}{\partial \hat{y}} \right) + \frac{m_3}{m_2} \frac{\partial \hat{W}u}{\partial \hat{z}} - \frac{U}{\rho G^{1/2}} PRC, \quad (4.5.2)$$

$$RU = \frac{m_1}{m_2} f_3 V - V \left(v \frac{m_1^2}{m_2^2} \frac{\partial m_2}{\partial \hat{x}} - u \frac{\partial m_1}{\partial \hat{y}} \right) + \text{DIF}U, \quad (4.5.3)$$

$$\frac{\partial V}{\partial t} + \frac{m_2}{m_1} \left(\frac{\partial P}{\partial \hat{y}} + \frac{\partial G^{23} P}{\partial \hat{z}} \right) = -\text{ADV}V + RV, \quad (4.5.4)$$

$$\text{ADV}V = m_2 \left(\frac{\partial U_V}{\partial \hat{x}} + \frac{\partial V_V}{\partial \hat{y}} \right) + \frac{m_3}{m_1} \frac{\partial \hat{W}_V}{\partial \hat{z}} - \frac{V}{\rho G^{1/2}} \text{PRC}, \quad (4.5.5)$$

$$RV = -\frac{m_2}{m_1} f_3 U - U \left(u \frac{m_2^2}{m_1^2} \frac{\partial m_1}{\partial \hat{y}} - v \frac{\partial m_2}{\partial \hat{x}} \right) + \text{DIF}V, \quad (4.5.6)$$

$$\frac{\partial W}{\partial t} + \frac{1}{m_3} \frac{\partial}{\partial \hat{z}} \left(\frac{P}{G^{1/2}} \right) + \sigma \frac{gP}{m_3 C_m^2} = \frac{1}{m_3} \text{BUOY} - \text{ADV}W + RW, \quad (4.5.7)$$

$$\text{BUOY} = \sigma \frac{\rho G^{1/2} \theta_m'}{\theta_m} g - (1 - \sigma) \rho' G^{1/2} g, \quad (4.5.8)$$

$$\text{ADV}W = \frac{m_1 m_2}{m_3} \left(\frac{\partial U_W}{\partial \hat{x}} + \frac{\partial V_W}{\partial \hat{y}} \right) + \frac{\partial \hat{W}_W}{\partial \hat{z}} - \frac{W}{\rho G^{1/2}} \text{PRC}, \quad (4.5.9)$$

$$RW = \text{DIF}W, \quad (4.5.10)$$

where

$$U = \frac{\rho G^{1/2}}{m_2} u, \quad V = \frac{\rho G^{1/2}}{m_1} v, \quad W = \frac{\rho G^{1/2}}{m_3} w, \quad (4.5.11)$$

$$\hat{w} = \frac{1}{G^{1/2}} (m_1 G^{1/2} G^{13} u + m_2 G^{1/2} G^{23} v + w), \quad (4.5.12)$$

$$\hat{W} = \frac{1}{G^{1/2}} \left\{ \frac{m_1 m_2}{m_3} (G^{1/2} G^{13} U + G^{1/2} G^{23} V + W) \right\}, \quad (4.5.13)$$

$$P = p' G^{1/2}. \quad (4.5.14)$$

Here, u , v and w are the velocity components, m_1 and m_2 are the map factors, m_3 is not a map factor in the z direction but a variable introduced for definition of momentum. ADVs are the advection terms and DIF.s are the diffusion terms. Symbols p' , ρ and g are the pressure perturbation from the hydrostatic state, density and gravity acceleration, respectively. $G^{1/2}$, G^{13} and G^{23} are the metric tensors, f and a are the Coriolis parameter and radius of the earth. Symbol σ is the switching parameter to choose the way to calculate the buoyancy term. Symbol θ_m is the mass-virtual potential temperature (Saito 1997) defined as

$$\theta_m \equiv \theta (1 + 0.608 q_v) (1 - q_c - q_i - q_r - q_s - q_g), \quad (4.5.15)$$

where q is the mixing ratios of water substances and subscripts v , c , i , r , s and g represent water vapor, cloud water, cloud ice, rain, snow and graupel, respectively. Symbol θ_m' is the perturbation of θ_m from 300 K. \hat{W} and \hat{w} are vertical momentum and vertical velocity along with \hat{z} coordinate.

In this model, density is defined by the sum of the masses of moist air and water substances per unit volume as

$$\begin{aligned}\rho &\equiv \rho_d + \rho_v + \rho_c + \rho_i + \rho_r + \rho_s + \rho_g \\ &= \rho_a + \rho_c + \rho_i + \rho_r + \rho_s + \rho_g,\end{aligned}\quad (4.5.16)$$

where ρ_a is the density of air.

PRC is the sum of fallout of precipitable water substances defined by

$$\text{PRC} = \frac{\partial}{\partial \hat{z}} \left(\rho_a V_r q_r + \rho_a V_s q_s + \rho_a V_g q_g \right), \quad (4.5.17)$$

where V_r, V_s, V_g are the terminal fall velocities of rain, snow and graupel, respectively.

In MSM0603, σ is set to zero and buoyancy term is calculated directly from the perturbation of density. The Lambert conformal projection is employed and the map factors and m_3 are given by

$$m_1 = m_2 = m = \left(\frac{\cos \varphi}{\cos \varphi_1} \right)^{c-1} \left(\frac{1 + \sin \varphi_1}{1 + \sin \varphi} \right)^c, \quad (4.5.18)$$

$$m_3 = 1, \quad (4.5.19)$$

where φ is the latitude of concerned point, $\varphi_1 = 60^\circ$, $\varphi_2 = 30^\circ$ and c is given by

$$c = \ln \left(\frac{\cos \varphi_1}{\cos \varphi_2} \right) / \ln \left[\frac{\tan \left(45^\circ - \frac{\varphi_1}{2} \right)}{\tan \left(45^\circ - \frac{\varphi_2}{2} \right)} \right]. \quad (4.5.20)$$

The terrain-following coordinate (Gal-Chen and Somerville 1975) is adopted and the vertical coordinate \hat{z} for the height z is given by

$$\hat{z} = \frac{H(z - z_s)}{H - z_s}, \quad (4.5.21)$$

where H is the model top height and z_s is the surface height. The metric tensors $G^{1/2}$, $G^{1/2}G^{13}$, $G^{1/2}G^{23}$ are defined by

$$G^{1/2} = 1 - \frac{z_s}{H}, \quad G^{1/2}G^{13} = \left(\frac{\hat{z}}{H} - 1 \right) \frac{\partial z_s}{\partial \hat{x}}, \quad G^{1/2}G^{23} = \left(\frac{\hat{z}}{H} - 1 \right) \frac{\partial z_s}{\partial \hat{y}}. \quad (4.5.22)$$

(a-2) Pressure equation

The pressure equation is described as follows.

$$\frac{\partial P}{\partial t} + C_m^{-2} (\text{DIVT} - \text{PRC} - \text{PFT}) = 0, \quad (4.5.23)$$

$$\text{DIVT} = m_1 m_2 \left(\frac{\partial U}{\partial \hat{x}} + \frac{\partial V}{\partial \hat{y}} \right) + m_3 \frac{\partial \hat{W}}{\partial \hat{z}}, \quad (4.5.24)$$

$$\text{PFT} = \frac{\rho G^{1/2}}{\theta_m} \frac{\partial \theta_m}{\partial t}. \quad (4.5.25)$$

Here, C_m is the velocity of sound waves defined by

$$C_m^2 = \frac{C_p}{C_v} R \theta_m \left(\frac{p}{p_0} \right)^{\frac{R}{C_p}}. \quad (4.5.26)$$

C_p . and C_v . are the specific heat dry air at constant pressure and constant volume, respectively. R is the gas constant for dry air and $p_0 = 1000\text{hPa}$ is a reference pressure. DIVT and PFT are the divergence in \hat{z} coordinate and the thermal expansion of air, respectively.

(a-3) Forecast equation of potential temperature

The thermodynamic equation is given by,

$$\frac{\partial \theta}{\partial t} = -\text{ADV} \theta + \frac{Q}{C_p \pi} + \text{DIF} \cdot \theta, \quad (4.5.27)$$

$$\text{ADV} \theta = \frac{1}{\rho G^{1/2}} \left\{ m_1 m_2 \left(\frac{\partial U \theta}{\partial \hat{x}} + \frac{\partial V \theta}{\partial \hat{y}} \right) + m_3 \frac{\partial \hat{W} \theta}{\partial \hat{z}} - \theta \text{DIVT} \right\}, \quad (4.5.28)$$

where Q is the diabatic heating. π is the Exner function defined by

$$\pi = \left(\frac{p}{p_0} \right)^{\frac{R}{C_p}}. \quad (4.5.29)$$

(a-4) Forecast equation of water substances

The forecast equations of mixing ratios of water substances are given by,

$$\frac{\partial q_n}{\partial t} = -\text{ADV} q_n + Q_n + \text{DIF} \cdot q_n, \quad (4.5.30)$$

$$\text{ADV} q_n = \frac{1}{\rho G^{1/2}} \left\{ m_1 m_2 \left(\frac{\partial U q_n}{\partial \hat{x}} + \frac{\partial V q_n}{\partial \hat{y}} \right) + m_3 \frac{\partial \hat{W} q_n}{\partial \hat{z}} - q_n \text{DIVT} \right\}. \quad (4.5.31)$$

(a-5) State equation

The state equation is

$$\rho = \frac{p_0}{R \theta_m} \left(\frac{p}{p_0} \right)^{\frac{C_v}{R}}. \quad (4.5.32)$$

b) Finite discretization

The grid structure of the model is the Arakawa C type in the horizontal direction and the Lorenz type in the vertical direction. The fourth-order finite difference scheme is employed to calculate horizontal advection terms, while the vertical advection is calculated by second order scheme. Considering the staggered grid structure, the fourth-order finite

difference are described by

$$\left. \frac{\partial \phi}{\partial x} \right|_i = \frac{9}{8} \frac{\phi_{i+1/2} - \phi_{i-1/2}}{\Delta x} - \frac{1}{8} \frac{\phi_{i+1+1/2} - \phi_{i-1-1/2}}{3\Delta x} + \frac{3}{640} (\Delta x)^4 \frac{\partial^5 \phi}{\partial x^5} + O[(\Delta x)^6]. \quad (4.5.33)$$

For advection of scalar prognostic variables, the fourth-order finite difference for a flux form is given by

$$\left. \frac{\partial U\theta}{\partial x} \right|_i = \frac{9}{8} \frac{(U\bar{\theta})_{i+1/2} - (U\bar{\theta})_{i-1/2}}{\Delta x} - \frac{1}{8} \frac{(U\bar{\theta})_{i+1+1/2} - (U\bar{\theta})_{i-1-1/2}}{3\Delta x}, \quad (4.5.34)$$

where second order interpolation process is used to calculate $\bar{\theta}_{i-1/2}$ at the vector point currently. For advection of vector variables,

$$\left. \frac{\partial Uu}{\partial x} \right|_{i+1/2} = \frac{9}{8} \frac{(U\bar{u})_{i+1} - (U\bar{u})_i}{\Delta x} - \frac{1}{8} \frac{(U\bar{u})_{i+2} - (U\bar{u})_{i-1}}{3\Delta x}, \quad (4.5.35)$$

The above higher-order schemes is employed with the modified centered difference advection scheme (Kato 1998), which is a kind of flux limiter and acts as a flux correction scheme.

c) Split explicit (HE-VI) scheme

For the time-splitting, horizontally explicit, and vertically implicit (HE-VI) scheme is used. Forward time integrations

$$\frac{U^{\tau+\Delta\tau} - U^\tau}{\Delta\tau} + \frac{m_1}{m_2} \left(\frac{\partial P^\tau}{\partial \hat{x}} + \frac{\partial G^{13} P^\tau}{\partial \hat{z}} \right) = -(\text{ADV}U - RU), \quad (4.5.36)$$

$$\frac{V^{\tau+\Delta\tau} - V^\tau}{\Delta\tau} + \frac{m_2}{m_1} \left(\frac{\partial P^\tau}{\partial \hat{y}} + \frac{\partial G^{23} P^\tau}{\partial \hat{z}} \right) = -(\text{ADV}V - RV), \quad (4.5.37)$$

are used for horizontal momentum equations, where $\Delta\tau$ is the short time step. Backward time integration is employed for vertical momentum equation as

$$\frac{\hat{W}^{\tau+\Delta\tau} - \hat{W}^\tau}{\Delta\tau} + \frac{1}{m_3} \frac{\partial}{\partial \hat{z}} \left(\frac{P^\beta}{G^{1/2}} \right) + \frac{gP^\beta}{m_3 C_m^2} = \frac{1}{m_3} \text{BUOY} - \text{ADV}W + RW + (1-\sigma) \frac{gP^\tau}{m_3 C_m^2}, \quad (4.5.38)$$

where

$$P^\beta = \frac{1+\beta}{2} P^{\tau+\Delta\tau} + \frac{1-\beta}{2} P^\tau. \quad (4.5.39)$$

The pressure equation is integrated backward as

$$\frac{P^{\tau+\Delta\tau} - P^\tau}{\Delta\tau} + C_m^2 \left\{ m_1 m_2 \left(\frac{\partial U^\gamma}{\partial \hat{x}} + \frac{\partial V^\gamma}{\partial \hat{y}} \right) + m_3 \frac{\partial \hat{W}^\beta}{\partial \hat{z}} - \text{PRC} - \text{PFT} \right\} = \text{DIF}.P, \quad (4.5.40)$$

where

$$U^\gamma = \frac{1+\gamma}{2} U^{\tau+\Delta\tau} + \frac{1-\gamma}{2} U^\tau, \quad V^\gamma = \frac{1+\gamma}{2} V^{\tau+\Delta\tau} + \frac{1-\gamma}{2} V^\tau, \quad \hat{W}^\beta = \frac{1+\beta}{2} \hat{W}^{\tau+\Delta\tau} + \frac{1-\beta}{2} \hat{W}^\tau. \quad (4.5.41)$$

Here, β and γ are the implicit factor. $\beta=1$ and $\gamma=1$ are employed in MSM0603.

Eliminating \hat{W}^β from the pressure equation (4.5.40) using the vertical momentum equation (4.5.38), we obtain the one dimensional Helmholtz type equation

$$-\left(\frac{C_m \Delta \tau (1 + \beta)}{2}\right)^2 \frac{\partial}{\partial \hat{z}} \left(\frac{1}{G^{1/2}} \frac{\partial}{\partial \hat{z}} \left(\frac{P^\beta}{G^{1/2}} \right) \right) - \left(\frac{C_m \Delta \tau (1 + \beta)}{2}\right)^2 \frac{\partial}{\partial \hat{z}} \left(\frac{g P^\beta}{C_m^2 G^{1/2}} \right) + P^\beta \quad (4.5.42)$$

$$= \text{FP.HE.INV} + \text{HP.HE.VAR}$$

where,

$$\text{FP.HE.INV} = C_m^2 \frac{\Delta \tau (1 + \beta)}{2} \left(\text{PRC}^t + \text{PFT}^t + \frac{\text{DIF} \cdot P^t}{C_m^2} \right) \quad (4.5.43)$$

$$- C_m^2 \left(\frac{\Delta \tau (1 + \beta)}{2} \right)^2 m_3 \frac{\partial}{\partial \hat{z}} \left\{ \frac{1}{G^{1/2}} \left(\frac{1}{m_3} \text{BUOY}^t - (\text{ADV}W^t - \text{RW}^t) + (1 - \sigma) \frac{g P^t}{m_3 C_m^2} \right) \right\}$$

FP.HE.VAR =

$$P^\tau - C_m^2 \frac{\Delta \tau (1 + \beta)}{2} \left\{ m_1 m_2 \left(\frac{\partial U^\gamma}{\partial \hat{x}} + \frac{\partial V^\gamma}{\partial \hat{y}} + \frac{\partial}{\partial \hat{z}} (G^{13} U^\beta + G^{23} V^\beta) \right) + m_3 \frac{\partial}{\partial \hat{z}} \frac{W^\tau}{G^{1/2}} \right\}. \quad (4.5.44)$$

Considering $(\hat{W}^{\tau+\Delta\tau} - \hat{W}^\tau) / \Delta\tau = 0$ at upper and lower boundary, upper and lower boundary conditions are given by

$$\frac{1}{G^{1/2}} \frac{\partial}{\partial \hat{z}} \left(\frac{P^\beta}{G^{1/2}} \right) + \frac{g P^\beta}{C_m^2 G^{1/2}} = \frac{m_3}{G^{1/2}} \left\{ \frac{1}{m_3} \text{BUOY}^t - \text{ADV}W^t + \text{RW}^t + (1 - \sigma) \frac{g P^t}{m_3 C_m^2} \right\}. \quad (4.5.45)$$

d) Divergence damping

An acoustic filter which is based on the idea of Skamarock and Klemp (1992) is implemented to avoid the computational instability by the sound waves. The gradient of the divergence is added to the momentum equation,

$$RU \rightarrow RU + \alpha_H \frac{m_1}{m_2} \left(\frac{\partial \text{DIVT}}{\partial \hat{x}} + \frac{\partial G^{13} \text{DIVT}}{\partial \hat{z}} \right), \quad (4.5.46)$$

$$RV \rightarrow RV + \alpha_H \frac{m_2}{m_1} \left(\frac{\partial \text{DIVT}}{\partial \hat{y}} + \frac{\partial G^{23} \text{DIVT}}{\partial \hat{z}} \right), \quad (4.5.47)$$

$$RW \rightarrow RW + \alpha_V \frac{1}{m_2} \frac{\partial}{\partial \hat{z}} \frac{\text{DIVT}}{G^{1/2}}, \quad (4.5.48)$$

where

$$\alpha_H = 0.06 \min \left[\left(\frac{\Delta x}{m_1} \right)^2, \left(\frac{\Delta y}{m_2} \right)^2 \right], \quad (4.5.49)$$

$$\alpha_V = 0.05 (G^{1/2} \Delta z)^2. \quad (4.5.50)$$

e) Time splitting of advection and gravity waves

To stabilize model integration of the cases where environmental wind is strong and strong inversion layer exists, a new time splitting scheme is implemented (Saito et. al., 2006). In the scheme, we fully evaluate higher-order advection terms with the modified advection scheme at the center of the leapfrog time step, and then adjust the lower-order

(second order) components at each short time step only in the latter half of the leapfrog time integration scheme,

$$ADV^* = ADV - ADVL + ADVL^\tau. \quad (4.5.51)$$

Here, ADV and ADVL are the higher-order advection and the lower-order advection component at a leapfrog time step, respectively, while $ADVL^\tau$ is the lower-order advection component at each short time step. This adjustment is done from $(ns-1)/2+1$ to $ns-1$, where ns is the ratio of $2\Delta t$ and $\Delta\tau$ as shown Fig. 4.5.1.

Using this adjustment, the equation of \hat{W} is rewritten as

$$\begin{aligned} \frac{\hat{W}^{\tau+\Delta\tau} - \hat{W}^\tau}{\Delta\tau} + \frac{1}{m_3} \frac{\partial}{\partial \hat{z}} \left(\frac{P^\beta}{G^{1/2}} \right) + \frac{gP^\beta}{m_3 C_m^2} \\ = \frac{1}{m_3} \text{BUOY} - (ADVW - ADVLW + ADVLW^\tau) + RW + (1-\sigma) \frac{gP^\tau}{m_3 C_m^2}. \end{aligned} \quad (4.5.52)$$

The time splitting of advection of potential temperature using this adjustment is an alternative way to split gravity waves

$$\frac{\theta^{\tau+\Delta\tau} - \theta^\tau}{\Delta\tau} = -(ADV\theta - ADVL\theta + ADVL\theta^\tau) + \frac{Q}{C_p \pi} + \text{DIF}\theta, \quad (4.5.53)$$

where $ADVL\theta$ is computed by a flux form second-order central difference.

f) Computational diffusion

A nonlinear damper, fourth order linear damper and the Asselin time filter (Robert, 1966) are employed to suppress the computational noise.

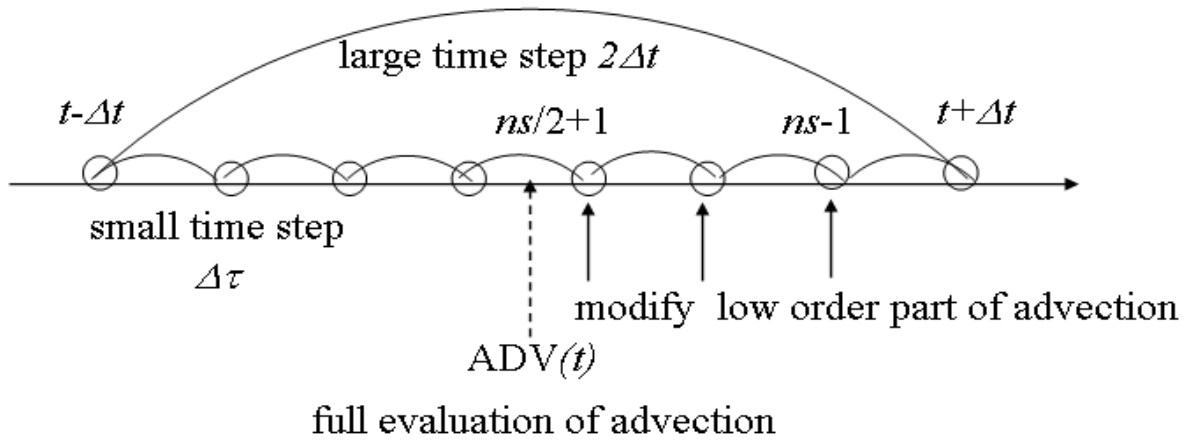


Fig. 4.5.1 Time split of advection for case of $ns = 2\Delta t / \Delta\tau = 7$, after Saito et al. (2006) Fig. 3.

(f-1) Nonlinear damper

Nonlinear damping (Nakamura, 1978),

$$D_{NL} = \frac{1}{8m_{NL}\Delta t} \left\{ (\Delta x)^3 \frac{\partial}{\partial x} \left(\left| \frac{\partial \phi}{\partial x} \right| \frac{\partial \phi}{\partial x} \right) + (\Delta y)^3 \frac{\partial}{\partial y} \left(\left| \frac{\partial \phi}{\partial y} \right| \frac{\partial \phi}{\partial y} \right) \right\}, \quad (4.5.54)$$

is added to the diffusion term of ϕ where $m_{NL} = 1200$ is used. For two-grid noise of amplitude a , 1/e-folding time is given by $m_{NL}\Delta t / a$. This nonlinear damping sometimes causes the computational instability because of the excessive diffusion. A limit is applied to D_{NL} using the estimated amplitude of the maximum wave number.

(f-2) Fourth order linear damper

Fourth order linear damping,

$$D_{2D} = \frac{1}{16m_{2D}\Delta t} \left\{ (\Delta x)^4 \frac{\partial^4 \phi}{\partial x^4} + (\Delta y)^4 \frac{\partial^4 \phi}{\partial y^4} \right\}, \quad (4.5.55)$$

is added to the diffusion term of ϕ where $m_{2D} = 600$ is used. 1/e-folding time is given by $m_{2D}\Delta t$.

(f-3) Asselin time filter

After the time integration, all quantities of prognostic variables are modified according to the Asselin time filter,

$$\phi(t) = \phi(t) + 0.5\nu \{ \phi(t - \Delta t) - 2\phi(t) + \phi(t + \Delta t) \}, \quad (4.5.56)$$

where ν is set to 0.2 in MSM0603.

g) Boundary conditions

(g-1) Lateral boundary conditions

Rayleigh damping,

$$D_R = -\frac{D_{xy}}{m_R} \{ \phi - \phi_{EXT} \}, \quad (4.5.57)$$

is added to the time tendency of all prognostic variables ϕ , where ϕ_{EXT} is the value of the external model. m_R is the coefficient which determines the 1/e-folding time and $m_R = 2400$ is used. D_{xy} is the function of location, where D_{xy} is unity at lateral boundary and decreases as the grid points are away from lateral boundary.

(g-2) Upper boundary

Rayleigh damping,

$$D_{RZ} = -\frac{D_z}{m_{RZ}} \{ \phi - \phi_{EXT} \}, \quad (4.5.58)$$

is added to the time tendency of all prognostic variables ϕ , where ϕ_{EXT} is the value of the external model. Symbol m_{RZ} is the coefficient which determines the 1/e-folding time and $m_{RZ} = 2400$ is used. D_z is the function of the number of the layers from the model top.

4.5.4 Cloud physics

A bulk parameterization of cloud microphysics based on Lin et al. (1983) is adopted (Ikawa and Saito, 1991). In the scheme, water substance is expressed by its mixing ratio and categorized into six forms: water vapor (q_v), cloud water (q_c), rain (q_r), cloud ice (q_i), snow (q_s) and graupel (q_g). The prognostic equations for mixing ratios and potential temperature θ are as follows:

$$\frac{\partial q_v}{\partial t} + \text{ADV}(q_v) - \text{DIF}(q_v) = P_{v_evp_r} - P_{i_dep_v} - P_{s_dep_v} - P_{g_dep_v} - P_{i_nud_v} - P_{w_cnd_v} \quad (4.5.59)$$

$$\begin{aligned} \frac{\partial q_c}{\partial t} + \text{ADV}(q_c) - \text{DIF}(q_c) = & - P_{r_aut_w} - P_{r_ac_r_w} + P_{w_cnd_v} - P_{i_frz_w} - P_{s_ac_s_w} - P_{g_ac_s_w} \\ & - P_{g_ac_g_w} + \delta P_{w_mlt_i} \end{aligned} \quad (4.5.60)$$

$$\begin{aligned} \frac{\partial q_r}{\partial t} + \text{ADV}(q_r) - \text{DIF}(q_r) = & - P_{r_prc_r} + P_{r_ac_r_w} + P_{r_aut_w} - P_{v_evp_r} - P_{g_frz_r} - P_{g_ac_i_r} \\ & - P_{s_ac_s_r} - P_{g_ac_s_r} - P_{g_ac_g_r} + \delta (P_{r_mlt_s} + P_{r_mlt_g}) \end{aligned} \quad (4.5.61)$$

$$\begin{aligned} \frac{\partial q_i}{\partial t} + \text{ADV}(q_i) - \text{DIF}(q_i) = & P_{i_nud_v} + P_{i_frz_w} + P_{i_dep_v} - P_{g_ac_r_i} - P_{s_ac_s_i} - P_{g_ac_g_i} \\ & - P_{s_aut_i} - \delta P_{w_mlt_i} \end{aligned} \quad (4.5.62)$$

$$\begin{aligned} \frac{\partial q_s}{\partial t} + \text{ADV}(q_s) - \text{DIF}(q_s) = & - P_{r_prc_s} + P_{s_dep_v} + P_{s_aut_i} + P_{s_ac_s_w} - P_{g_cn_w_s} + P_{s_ac_s_i} \\ & + P_{s_ac_s_r} - P_{g_ac_r_s} - P_{g_ac_g_s} - \delta P_{r_mlt_s} \end{aligned} \quad (4.5.63)$$

$$\begin{aligned} \frac{\partial q_g}{\partial t} + \text{ADV}(q_g) - \text{DIF}(q_g) = & - P_{r_prc_g} + P_{g_dep_v} + P_{g_cn_w_s} + P_{g_ac_s_w} + P_{g_ac_g_r} + P_{g_ac_g_s} \\ & + P_{g_ac_g_w} + P_{g_ac_g_i} + P_{g_ac_i_r} + P_{g_ac_r_i} + P_{g_ac_s_r} + P_{g_ac_r_s} + P_{g_frz_r} \\ & - \delta P_{r_mlt_g} \end{aligned} \quad (4.5.64)$$

$$\begin{aligned} \frac{\partial \theta}{\partial t} + \text{ADV}(\theta) - \text{DIF}(\theta) = & - \frac{L_v}{c_p \pi} (P_{v_evp_r} - P_{w_cnd_v}) \\ & + \frac{L_s}{c_p \pi} (P_{i_dep_v} + P_{i_nud_v} + P_{s_dep_v} + P_{g_dep_v}) \\ & + \frac{L_f}{c_p \pi} (P_{s_ac_s_w} + P_{g_ac_s_w} + P_{g_ac_g_w} + P_{g_ac_i_r} + P_{i_frz_w}) \\ & + \frac{L_f}{c_p \pi} [P_{s_ac_s_r} + P_{g_ac_s_r} + P_{g_ac_g_r} - \delta (P_{w_mlt_i} + P_{r_mlt_s} + P_{r_mlt_g})] \end{aligned} \quad (4.5.65)$$

where t is time, $\text{ADV}(x)$ the advection term of x and $\text{DIF}(x)$ the diffusion term of x . The symbols L_v , L_s and L_f are latent heat of vaporization, sublimation and fusion, respectively; c_p the specific heat of dry air at constant pressure, π the non-dimensional pressure (Exner function), and $\delta = 1$ when the temperature is above 0 deg C and $\delta = 0$ otherwise. The symbol $P_{x_proc_y}$ denotes the production rate of water substance x (v: water vapor, w: cloud water, r: rain, i: cloud ice, s: snow, g: graupel) through the process $proc$ (ac: accretion, aut: autoconversion,

cn: conversion such as riming, cnd: condensation, dep: depositional growth or evaporation, evp: evaporation, frz: freezing, mlt: melting, nud: nucleation by deposition) concerning water substance y , $Px_{proc_y_z}$ denotes the production rate of water substance x through the process $proc$ concerning water substances y and z , and P_prc_x denotes precipitation of x . In the following, Lnn and $ISnn$ denote the number of equation appearing in Lin et al. (1983) and Ikawa and Saito (1991). The production rate terms are parameterized as follows:

- # $Pg_ac_g_i$: accretion of cloud ice by graupel, the same as $Pgaci$ in L41
- # $Pg_ac_g_r$: accretion of rain by graupel, the same as $Pgacr$ in L42 except that the approximation of differential velocity is modified as $|U_{Dr}(D_r) - U_{Dg}(D_g)| \cong \sqrt{(1.3\bar{U}_r - 1.0\bar{U}_g)^2 + 0.17\bar{U}_r\bar{U}_g}$, where $U_{Dr}(D_r)$ is the terminal velocity of rain of diameter D_r , \bar{U}_r is the mass-weighted mean terminal velocity of rain, $U_{Dg}(D_g)$ is the terminal velocity of graupel of diameter D_g and \bar{U}_g is the mass-weighted mean terminal velocity of graupel
- # $Pg_ac_g_s$: accretion of snow by graupel, the same as $Pgacs$ in L29 except that the approximation of differential velocity is modified as $|U_{Ds}(D_s) - U_{Dg}(D_g)| \cong \sqrt{(1.2\bar{U}_s - 0.95\bar{U}_g)^2 + 0.08\bar{U}_s\bar{U}_g}$, where $U_{Ds}(D_s)$ is the terminal velocity of snow of diameter D_s and \bar{U}_s is the mass-weighted mean terminal velocity of snow
- # $Pg_ac_g_w$: accretion of cloud water by graupel, the same as $Pgacw$ in L40
- # $Pg_ac_i_r$: portion of accretion of rain by cloud ice which is converted into graupel, the same as $Piacr$ in L26 except for the expression of fall velocity of rain
- # $Pg_ac_r_i$: portion of accretion of cloud ice by rain which is converted into graupel, the same as $Praci$ in L25 except for the expression of fall velocity of rain
- # $Pg_ac_r_s$: portion of accretion of snow by rain which is converted into graupel, the same as $Pg.racs$ in IS11-63
- # $Pg_ac_s_r$: portion of accretion of rain by snow which is converted into graupel, the same as $Pg.sacr$ in IS11-61
- # $Pg_ac_s_w$: portion of accretion of cloud water by snow which is converted into graupel, calculated as $Pg_ac_s_w = \left\{1 - \sqrt{\bar{D}_s/\bar{D}_{s0}}(q_{c0}/q_c)\right\}Psacw$, where \bar{D}_s is the mass-weighted mean diameter of snow, $\bar{D}_{s0} = 2.0 \times 10^{-4}$ m, $q_{c0} = 5.0 \times 10^{-4}$ kg/kg and $Psacw$ is the same as that in L24
- # $Pg_cn_w_s$: riming of snow by graupel, the same as $Pscng$ in IS11-54
- # Pg_dep_v : depositional growth (> 0) or evaporation (< 0) of graupel, the same as $Pgdep$ in IS11-33
- # Pg_frz_r : freezing of rain to form graupel, the same as $Pgfrz$ in L45
- # Pi_dep_v : depositional growth (> 0) or evaporation (< 0) of cloud ice, the same as $Pidep$ in IS11-24 except that a number concentration of cloud ice is diagnosed from the temperature and supersaturation ratio over ice

- # Pi_frz_w : freezing of cloud water to form cloud ice, the same as Pifzc in IS11-20
- # Pi_nud_v : nucleation of cloud ice, calculated as $Pi_nud_v = [m_{i0} \exp\{a + b(S_i - 1)\} / (\rho - q_i)] / (2\Delta t)$, where m_{i0} is the mass of smallest ice particle, S_i the supersaturation ratio over ice, ρ the density of air, Δt the step of time integration, $a = 5.17$ and $b = 15.25$
- # Pr_ac_r_w : accretion of cloud water by rain, the same as Pracw in L51 except for the expression of fall velocity of rain
- # Pr_aut_w : collision and coalescence of cloud water to form rain (autoconversion), the same as Pccnr in IS11-75
- # Pr_mlt_g : melting of graupel to form rain, the same as Pgmelt in L47
- # Pr_mlt_s : melting of snow to form rain, the same as Psmlt in L32
- # Ps_ac_s_i : accretion of cloud ice by snow, the same as Psaci in L22
- # Ps_ac_s_r : portion of accretion of rain by snow which is consumed for the growth of snow, the same as Ps.sacr in IS11-64
- # Ps_ac_s_w : portion of accretion of cloud water by snow which is consumed for riming growth of snow, calculated as $Ps_ac_s_w = Psacw - Pg_ac_s_r$, where Psacw is the same as that in L24 except that the approximation of differential velocity is modified as $|U_{Ds}(D_s) - U_{Dr}(D_r)| \cong \sqrt{(1.2\bar{U}_s - 0.95\bar{U}_s)^2 + 0.08\bar{U}_s\bar{U}_r}$
- # Ps_aut_i : aggrigation of cloud ice to form snow (autoconversion), the same as Psaut in L21
- # Ps_dep_v : depositional growth (> 0) or evaporation (< 0) of snow, the same as Psdep in IS11-33 and IS11-34
- # Pv_evpr : evaporation of rain, the same as Prevp in L52
- # Pw_cnd_v : condensation of water vapor to form cloud water (saturation adjustment), the same as Pccnd in IS11-74
- # Pw_mlt_i : melting of cloud ice to form cloud water (cloud ice is assumed to melt into cloud water instantaneously above the freezing point)

Falling of rain and graupel is calculated using the box-Lagrangian scheme (Kato, 1995) to keep computational stability, by which the total amount in a vertical grid box is dropped while keeping terminal velocity constant during a time step interval and partitioned into grid boxes existing in the space where it is dropped.

4.5.5 Convective parameterization

The Kain-Fritsch (KF) convective parameterization scheme is adopted to represent the effects of subgrid-scale convection. Most assumptions in the KF scheme such as closure are the same as that used in the Fritsch-Chapell scheme

(Fritsch and Chappell, 1980). Some improvements in a cloud model and detrainment effects have been added to the KF scheme (Kain and Fritsch, 1990), and the further updated version (Kain, 2004) is implemented to MSM.

The source codes of the KF scheme have been originally developed for the Weather Research and Forecast (WRF) modeling system and implemented to MSM with consent of Dr. Kain in April 2002.

(a) Trigger function

To identify source layers for convective clouds, the KF scheme utilizes a trigger function based on the temperature of the lifting condensation level (LCL) and the grid-scale vertical velocity. As a first measure of initiation of parameterized convection, the potential updraft source layer (USL) of the lowest 50-hPa depth is lifted adiabatically to its LCL. A temperature perturbation based on the grid-scale vertical velocity (ΔT_{vLCL}) is added to the virtual temperature of the USL lifted at the LCL (T_{vLCL}) and then the trigger function $T_{vLCL} + \Delta T_{vLCL}$ is compared with the environmental virtual temperature (T_{vENV}) represented by a grid-scale value. If $T_{vLCL} + \Delta T_{vLCL} > T_{vENV}$ is met, the USL is regarded to have buoyancy and parameterized convection is initiated at the LCL. If not, the base of the potential USL is moved up one model layer and the comparison between trigger function and T_{vENV} is repeated while the base of the potential USL is below the lowest 300 hPa of the atmosphere.

While the vertical velocity at the LCL of one model grid is adopted as a temperature perturbation ΔT_{vLCL} for the KF scheme in the WRF model, the horizontally-averaged vertical velocity of the grid and surrounding eight grids is adopted in MSM.

(b) Mass flux formulation

The KF scheme utilizes a simple cloud model with a one-dimensional convective updraft and downdraft set, which is mass-conservative and allows cloud and environmental interaction. A convective updraft in the KF scheme is represented using a steady-state entraining/detraining plume model, where equivalent potential temperature and water vapor are both entrained and detrained at each level of height. High entrainment rate is favored by high parcel buoyancy and moist environment. On the other hand, high detrainment rate is favored by low parcel buoyancy and dry environment. Various hydrometers are detrained to the grid-scale prognostic equations and precipitate on the surface as a feedback of the KF scheme. A portion of the precipitation is calculated using the Kessler type conversion scheme in MSM.

If parameterized convection is triggered, the mass flux of the updraft is calculated using the radius of the updraft. The radius is rendered as a function of larger-scale forcing through the grid-resolvable vertical velocity of the updraft and the buoyancy variations are induced by the turbulent mixing between cloud and environment. The calculation of mixing uses a radius of updraft to modulate updraft entrainment and detrainment rates.

A parameterized downdraft is fueled by evaporation of condensate that is generated within the updraft. The convective downdraft starts at the layer 150 hPa above the LCL. Entrainment between the downdraft and environment is allowed only above the LCL and detrainment only below the LCL.

Parameterized shallow convection is allowed for any updraft that does not reach the minimum cloud depth for deep

convection. The minimum value of cloud depth is a function of temperature at cloud base.

(c) Closure assumption

Parameterized convection calculated by the KF scheme rearranges the mass in a column using the updraft, downdraft and environmental mass fluxes until the convective available potential energy (CAPE) is removed at least 85 % of the initial value. Once convection is triggered, CAPE is assumed to be removed in a grid column by the combined effects of lowering equivalent potential temperature in the USL and warming the environment aloft by compensating subsidence within an advective time period.

4.5.6 Radiation

(a) Longwave radiation

The basic framework of the longwave radiation fluxes and cooling rate computations follows Sugi et al. (1990). Longwave radiation is treated by a broad-band flux emissivity method for four spectral bands shown in Fig. 4.5.3.

Assuming a non-scattering atmosphere, the net longwave radiation flux F can be given by

$$F(z) = C(z, 0) \tau(s, T_{bottom}) \{ \pi B(T_{ground}) - \pi B(T_{bottom}) \} + C(z, \infty) \tau(s_{top} - s, T_{top}) \pi B(T_{top}) + \int_{top}^{bottom} C(z, z') \tau^*(|s - s'|, T') \frac{\partial \pi B(T')}{\partial T'} dT', \quad (4.5.66)$$

where $\tau(s, T)$ is the band transmissivity through an absorber s and $B(T)$ the total Planck function. $C(z, z')$ is the clear sky fraction between z and z' derived from the fractional cloud covers with the assumption of maximum-random cloud overlap. Clouds are treated as blackbodies, so that the effective fraction of semi-transparent cloud is given by the product of the cloud fraction by the emissivity (Kiehl and Zender, 1995).

The band transmissivity has the temperature dependence because of the Planck function $B_\nu(T)$. Two normalized band transmissivities are used for each absorber in a given spectral region $\Delta\nu$:

$$\tau(s, T) \equiv \int_{\Delta\nu} \tau_\nu(s) B_\nu(T) d\nu / \int_{\Delta\nu} B_\nu(T) d\nu, \quad (4.5.67)$$

$$\tau^*(s, T) \equiv \int_{\Delta\nu} \tau_\nu(s) \frac{\partial B_\nu(T)}{\partial T} d\nu / \int_{\Delta\nu} \frac{\partial B_\nu(T)}{\partial T} d\nu. \quad (4.5.68)$$

Over four spectral regions, the band transmissivities are evaluated with the help of transmission functions pre-calculated from the random model of Goody (1952). Absorption data of gases are derived from Rodgers and Walshaw (1966) for water vapor, Goldman and Kyle (1968) for ozone and Houghton (1977) for carbon dioxide (summarized in Roewe and

Liou, 1978). The e-type continuum absorption by water vapor is treated after the method of Roberts et al. (1976).

Considering the pressure broadening of the lines, the path length is given by the pressure weighted absorber amount

$$\tilde{s} = 1.66 \int_0^s (p/p_0)^n ds, \quad (4.5.69)$$

where p_0 is a reference pressure and n the pressure scaling parameter of each absorber. The diffusivity factor of 1.66 in Eq. (4.5.69) is used to approximate the integration over the direction of the radiance transmission. The transmission is calculated in each band shown in Fig. 4.5.3 and combined to yield the total transmissivity including overlapping effects of different absorbers.

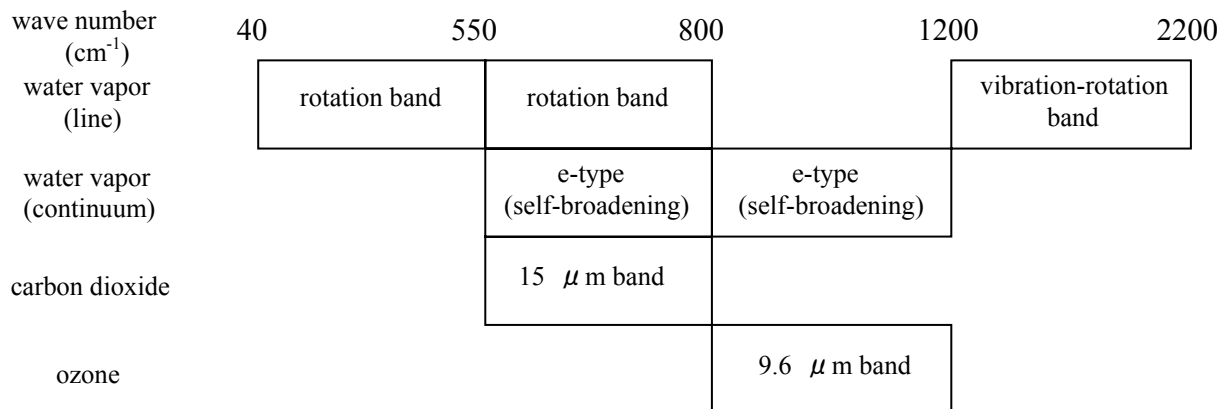


Fig. 4.5.3 Spectral regions for evaluation of broad-band transmissivities.

(b) Shortwave radiation

Most of the shortwave radiation scheme is the same as that of GSM (4.2.3, Kitagawa, 2000), except that the spectrum is divided into 18 bands by method of Briegleb (1992) using the k -distribution method. Spectral regions and absorbers of shortwave radiation are shown in Fig. 4.5.4.

(c) Radiatively active constituents

Radiatively active gases are prognostic water vapor, globally uniform carbon dioxide (at 375ppmv) and oxygen (at 209 490ppmv). The cloud fraction at each level is obtained by an empirical relation between the cloud fraction and the relative humidity (Ohno and Isa, 1984), while the cloud fraction below 500 m is set to zero. Cloud water and ice content are diagnosed from the precipitable water amount by the method of Hack (1998). The effective radius of the cloud liquid droplets is fixed at 15 micrometers, while the effective radius of the ice crystals varies in the range 20–150 microns according to the temperature (Ou and Liou, 1995). The concentration and optical properties of aerosols are specified as the continental and maritime types of background values without seasonal variation (Kitagawa, 2000).

(d) Time and horizontal resolution of the radiation calculation

The longwave and shortwave radiation are calculated every 900 seconds on a coarser (reduced radiation) grid to reduce the computational costs. The longwave radiation is modified by the surface temperature and the shortwave radiation by the solar zenith angle at every time step.

band	1-7	8	9-18				
wavelength interval (μ m)	0.20-0.35	0.35-0.70	0.70-2.63	2.63-2.86	2.86-4.16	4.16-4.55	4.55-5.00
water vapor			weak lines and strong lines (7 bands)				
oxygen		B-band	A-band				
carbon dioxide				2.7 μ -band		4.3 μ -band	
ozone	Hartley-Huggins band	Chappius band					
air molecule	Rayleigh scattering						
aerosol	Mie scattering and absorption (two types of climatological aerosols)						
cloud droplet	Mie scattering and absorption (distinguished into water droplets and ice particles)						

Fig. 4.5.4 Spectral regions and absorbers of shortwave radiation

4.5.7 Vertical turbulent diffusion

The effects of turbulence are represented as physical diffusion. The final products of turbulent diffusion process are the diffusion coefficients K_m for momentum and K_h for potential temperature and moisture. They are related with turbulence kinetic energy(TKE) E and mixing length l such that

$$K_m = C_m l E^{\frac{1}{2}}, \quad K_h = \text{Pr}^{-1} K_m, \quad (4.5.70)$$

where C_m is a constant and Pr is the Prandtl number.

Equation of TKE is based on Klemp and Wilhelmson (1978):

$$\frac{\partial E}{\partial t} = -\text{ADV}.E - \overline{\theta'w'} \frac{\partial \theta}{\partial z} - \sum_{i,j} \overline{u_i' u_j'} \frac{\partial u_i}{\partial x_j} - \frac{C_e E^{\frac{3}{2}}}{l} + \text{DIF}.E, \quad (4.5.71)$$

where Reynolds stress $\overline{u_i' u_j'}$ and buoyancy flux $\overline{\theta'w'}$ are displayed as:

$$\overline{u_i' u_j'} = -K_m \left(\frac{\partial u_i}{\partial x_j} + \frac{\partial u_j}{\partial x_i} \right) + \frac{2}{3} \delta_{ij} E, \quad \overline{\theta' w'} = -K_h \frac{\partial \theta}{\partial z}. \quad (4.5.72)$$

By substituting K_h at (4.5.70), and $\overline{u_i' u_j'}$ and $\overline{\theta' w'}$ at (4.5.72) into (4.5.71), and omitting time differential, advection, diffusion, and divergence terms as small from this equation, K_m and E are diagnosed as follows:

$$K_m^2 = \frac{C_m^3}{C_e} l^4 \left[\sum_{i,j} \left(\frac{\partial u_i}{\partial x_j} + \frac{\partial u_j}{\partial x_i} \right) \frac{\partial u_i}{\partial x_j} - \frac{g}{\theta} \frac{1}{\text{Pr}} \frac{\partial \theta}{\partial z} \right], \quad E = \left(\frac{K_m}{C_m l} \right)^2. \quad (4.5.73)$$

C_m , C_e and Pr are set as:

$$C_m = \begin{cases} 0.2 & (z \leq h_{\text{PBL}}) \\ 0.1 & (z > h_{\text{PBL}}) \end{cases}, \quad C_e = 0.41, \quad \text{Pr} = \frac{1}{1 + 2 \frac{l}{\Delta z}}, \quad (4.5.74)$$

where h_{PBL} is the height of planetary boundary layer diagnosed by vertical profile of virtual potential temperature.

The mixing length l is given by:

$$l = \begin{cases} l_{\text{SC}}(z) & (z \leq h_{\text{PBL}}) \\ \Delta z & (z > h_{\text{PBL}}, N^2 \leq 0), \\ \min \left(\Delta z, 0.76 E^{\frac{1}{2}} / N \right) & (z > h_{\text{PBL}}, N^2 > 0) \end{cases}, \quad (4.5.75)$$

where

$$l_{\text{SC}}(z) = 0.25 \left[1.8 h_{\text{PBL}} \left\{ 1 - \exp \left(-4 \frac{z}{h_{\text{PBL}}} \right) - 0.0003 \exp \left(8 \frac{z}{h_{\text{PBL}}} \right) \right\} \right], \quad N^2 = \frac{g}{\theta} \frac{\partial \theta_l}{\partial z}, \quad \theta_l = \theta - \frac{L}{c_p \pi} q_c, \quad (4.5.76)$$

L is latent heat of vaporization, c_p is specific heat at constant pressure and q_c is mixing ratio of cloud water. $l_{\text{SC}}(z)$ is according to Sun and Chang (1986), and non-local like effect is introduced with it.

Vertical diffusion is treated implicitly so that diffusion coefficient cannot be restricted by Δz . The prognostic equation of diffusion for ϕ can be discretized in time as following:

$$\frac{\phi^{t+\Delta t} - \phi^{t-\Delta t}}{2\Delta t} = \nabla_H (K \nabla_H \phi^{t-\Delta t}) + \frac{\partial}{\partial z} \left(K \frac{\partial \phi^{t+\Delta t}}{\partial z} \right). \quad (4.5.77)$$

$\phi^{t+\Delta t}$ is obtained by solving this elliptic equation, and the tendency by diffusion is evaluated by the left side of it with known $\phi^{t-\Delta t}$ and obtained $\phi^{t+\Delta t}$.

4.5.8 Surface processes

The main procedures around surface processes are evaluating surface fluxes. They are calculated by bulk coefficient scheme such as:

$$\begin{aligned}\overline{u'w'} &= -C_m U_a u_a, & \overline{v'w'} &= -C_m U_a v_a, \\ \overline{\theta'w'} &= -C_h U_a (\theta_a - \theta_s), & \overline{q_v'w'} &= -C_q U_a (q_{va} - q_{vs}),\end{aligned}\quad (4.5.78)$$

in which bulk coefficients C_m , C_h , C_q on land are based on Louis et al. (1982):

$$C_m = \begin{cases} a_m^2 \left(\frac{1}{1 + \frac{2b\text{Ri}_B}{\sqrt{1+d\text{Ri}_B}}} \right) & (\text{Ri}_B \geq 0) \\ a_m^2 \left(1 - \frac{2b\text{Ri}_B}{1 + 3bca_m^2 \sqrt{\frac{z_a}{z_{0m}} |\text{Ri}_B|}} \right) & (\text{Ri}_B < 0) \end{cases}, \quad C_h = \begin{cases} a_m a_h \left(\frac{1}{1 + 3b\text{Ri}_B \sqrt{1+d\text{Ri}_B}} \right) & (\text{Ri}_B \geq 0) \\ a_m a_h \left(1 - \frac{3b\text{Ri}_B}{1 + 3bca_m a_h \sqrt{\frac{z_a}{z_{0h}} |\text{Ri}_B|}} \right) & (\text{Ri}_B < 0) \end{cases}, \quad (4.5.79)$$

where z_{0m} , z_{0h} are the roughness for momentum and the one for heat and moisture respectively, which are set based on the land use of each grid point. Ri_B is the bulk Richardson Number defined by

$$\text{Ri}_B = \frac{gz_a}{\frac{1}{2}(\theta_a + \theta_s)} \frac{(\theta_a - \theta_s)}{U_a^2}, \quad (4.5.80)$$

and

$$a_m = \frac{\kappa}{\log \frac{z_a}{z_{0m}}}, \quad a_h = \frac{\kappa}{\log \frac{z_a}{z_{0h}}}, \quad U_a = \sqrt{u_a^2 + v_a^2}. \quad (4.5.81)$$

Suffixes “a” and “s” indicate the lowest layer of atmosphere and surface respectively. Some constants are set such as $b = c = d = 5$, $\kappa = 0.4$ (von Karman constant). The bulk coefficient for moisture C_q is set to equal to C_h .

An effect of a stomatal resistance is introduced as following. The surface flux of moisture $\overline{q_v'w'}$ is represented with a resistance coefficient r_a ,

$$\overline{q_v'w'} = -\frac{1}{r_a} (q_{va} - q_{vs}), \quad r_a \equiv \frac{1}{C_q U_a}. \quad (4.5.82)$$

With an effect of a stomatal resistance, r_a is corrected by $r_a + r_s$, where r_s is a stomatal resistance. r_s is represented shortwave radiation flux towards surface S with as

$$r_s = r_{s,\text{day}} + \frac{r_{s,\text{night}}}{1 + \frac{S}{S_0}}, \quad (4.5.83)$$

where $S_0 = 1 \text{ W/m}^2$, $r_{s,\text{day}}$ is set to 30 sm^{-1} from April to October and 60 sm^{-1} in other month, and $r_{s,\text{night}} = 300 \text{ sm}^{-1}$.

The bulk coefficients on sea are based on Kondo (1975):

$$\begin{aligned} C_m &= 10^{-3} A_m [a_m + b_m u_{10}^{p_m}], \\ C_h &= 10^{-3} A_h [a_h + b_h u_{10}^{p_h} + c_h (u_{10} - 8)^2], \\ C_q &= 10^{-3} A_q [a_q + b_q u_{10}^{p_q} + c_q (u_{10} - 8)^2], \end{aligned} \quad (4.5.84)$$

where u_{10} is wind velocity at 10m, and values of constants are displayed at Table 4.5.1. A_m , A_h and A_q depend on a stability parameter defined by:

$$S = S_0 \frac{|S_0|}{|S_0| + 0.01}, \quad \text{where } S_0 = (\theta_s - \theta_a) u^{-2} [1 + \log_{10}(10/z)]^{-2}. \quad (4.5.85)$$

For stable condition (i.e. $\theta_a - \theta_s > 0$),

$$A_m = A_h = A_q = \begin{cases} 0.1 + 0.03S + 0.9 \exp(4.8S) & (-3.3 < S < 0) \\ 0 & (S \leq -3.3) \end{cases}, \quad (4.5.86)$$

and for unstable condition (i.e. $\theta_a - \theta_s \leq 0$),

$$A_m = 1 + 0.47S^{0.5}, \quad A_h = A_q = 1 + 0.64S^{0.5}. \quad (4.5.87)$$

Although roughness on land is set as to land use, that on sea is diagnosed by

$$\begin{aligned} z_{0m} &= \exp[\ln 10 - \kappa(C_m / A_m)^{-1/2}] \\ z_{0h} &= \exp[\ln 10 - \kappa(C_m / A_m)^{1/2} (C_h / A_h)^{-1}] \\ z_{0q} &= \exp[\ln 10 - \kappa(C_m / A_m)^{1/2} (C_q / A_q)^{-1}] \end{aligned} \quad (4.5.88)$$

Table 1: Constants included in bulk coefficient on sea

$u_{10}(\text{ms}^{-1})$	a_m	a_h	a_q	b_m	b_h	b_q	c_h	c_q	p_m	p_h	p_q
0.3 ~ 2.2	0	0	0	1.08	1.185	1.23	0	0	-0.15	-0.157	-0.16
2.2 ~ 5	0.771	0.927	0.969	0.0858	0.0546	0.0521	0	0	1	1	1
5 ~ 8	0.867	1.15	1.18	0.0667	0.01	0.01	0	0	1	1	1
8 ~ 25	1.2	1.17	1.196	0.025	0.0075	0.008	-0.00045	-0.0004	1	1	1
25 ~ 50	0	1.652	1.68	0.073	-0.017	-0.016	0	0	1	1	1

The bulk coefficients are also used in diagnosing surface physical quantities such as wind at 10m height, temperature and dew point at 1.5m height with values on the lowest layer of atmosphere and surface. Wind velocity at 10m height u_{10} , virtual potential temperature at 1.5m height $\theta_{v,1.5}$ are diagnosed by:

$$u_{10} = \sqrt{\frac{C_m(z_a)}{C_m(10)}} u_a, \quad \theta_{v1.5} = \theta_{vs} + \frac{C_h(z_a)}{C_h(1.5)} \sqrt{\frac{C_m(1.5)}{C_m(z_a)}} (\theta_{va} - \theta_{vs}). \quad (4.5.89)$$

On land, C_m and C_h in these equations are not based on Louis et al. (1982) previously described, but the universal functions by Beljaars and Holtslag (1991). The integrated universal functions Ψ_m and Ψ_h are given as the functions of $\zeta = z/L$,

$$\Psi_m(\zeta) = \begin{cases} -b\left(\zeta - \frac{c}{d}\right) \exp(-d\zeta) - a\zeta - \frac{bc}{d} & (\zeta \geq 0) \\ \frac{\pi}{2} - 2 \tan^{-1} x + \log \frac{(1+x)^2(1+x^2)}{8} & (\zeta < 0) \end{cases}, \quad (4.5.90)$$

$$\Psi_h(\zeta) = \begin{cases} -b\left(\zeta - \frac{c}{d}\right) \exp(-d\zeta) - \left(1 + \frac{2}{3}a\zeta\right)^{\frac{3}{2}} - \frac{bc}{d} + 1 & (\zeta \geq 0) \\ 2 \log \frac{1+x^2}{2} & (\zeta < 0) \end{cases},$$

where L is Monin-Obukov Length, and

$$a = 1, \quad b = \frac{2}{3}, \quad c = 5, \quad d = 0.35, \quad x = (1 - 16\zeta)^{\frac{1}{4}}.$$

C_m and C_h are represented with $\Phi_m(z, L)$ and $\Phi_h(z, L)$ as:

$$C_m = \frac{\kappa^2}{\Phi_m(z, L)^2}, \quad C_h = \frac{\kappa^2}{\Phi_m(z, L)\Phi_h(z, L)}, \quad (4.5.91)$$

where

$$\Phi_m(z, L) = \ln \frac{z-d}{z_{0m}} - \Psi_m\left(\frac{z-d}{L}\right) + \Psi_m\left(\frac{z_{0m}}{L}\right),$$

$$\Phi_h(z, L) = \ln \frac{z-d}{z_{0h}} - \Psi_h\left(\frac{z-d}{L}\right) + \Psi_h\left(\frac{z_{0h}}{L}\right), \quad (4.5.92)$$

and d is the zero-plane displacement (In MSM, $d = 0$).

To calculate $\Phi_m(z, L)$ and $\Phi_h(z, L)$, the value of L is needed. L satisfies the following equation,

$$Ri_B(z) = \frac{z}{L} \frac{\Phi_h(z, L)}{\Phi_m(z, L)^2}, \quad (4.5.93)$$

which can be solved by iteration method such as Newton's.

4.5.9 Ground temperature model

Ground temperature, which is used in evaluating surface fluxes and surface temperature, is predicted by 4-layer model. The basic equation is the conduction equation of heat, in which predicted variables are temperature T and heat

flux G ,

$$\rho_c \frac{\partial T}{\partial t} = -\frac{\partial G}{\partial z}, \quad G = -\lambda \frac{\partial T}{\partial z}, \quad (4.5.94)$$

where ρ_c and λ are the heat capacity and the coefficient of the thermal conductivity, respectively. By discretizing on vertical coordinate of N layers,

$$G_k = -2\lambda \frac{T_k - T_{k-1}}{\Delta z_k + \Delta z_{k-1}} \quad (k = 2, \dots, N), \quad \frac{\partial T_k}{\partial t} = -\frac{G_{k+1} - G_k}{\rho_c \Delta z_k} \quad (k = 1, \dots, N-1), \quad (4.5.95)$$

where $N = 4$ in MSM, Δz_k denotes thickness of k -th layer (concretely $\Delta z_1 = 0.04$, $\Delta z_2 = 0.15$, $\Delta z_3 = 0.4$ and $\Delta z_4 = 0.6$), and G_h ($k \geq 2$) give the flux by the slope of temperature between k -th and $(k+1)$ -th layer. G_1 is the heat flux towards surface, which is given by:

$$G_1 = S_{\downarrow} + L_{\downarrow} - H - E - \sigma T_1^4, \quad (4.5.96)$$

where S_{\downarrow} and L_{\downarrow} denote flux of shortwave and long-wave radiation towards surface, H and E represent flux of sensible heat and latent heat from surface, and σ is the Stefan-Boltzmann constant. G_k ($k \geq 2$) can be eliminated as:

$$\frac{\partial T_1}{\partial t} = \frac{G_1}{\rho_c \Delta z_1} + \frac{2\nu(T_2 - T_1)}{\Delta z_1(\Delta z_2 + \Delta z_1)}, \quad \frac{\partial T_k}{\partial t} = -\frac{2\nu(T_k - T_{k-1})}{\Delta z_k(\Delta z_k + \Delta z_{k-1})} + \frac{2\nu(T_{k+1} - T_k)}{\Delta z_k(\Delta z_{k+1} + \Delta z_k)} \quad (k = 2, \dots, N) \quad (4.5.97)$$

where $\nu \equiv \lambda / \rho_c$.

For time integration, the trapezoidal implicit method is adopted. Discretized equations on time are:

$$\begin{aligned} T_1^{n+1} &= T_1^n + \frac{\Delta t}{2} \left[\frac{G_1^{n+1} + G_1^n}{\rho_c \Delta z_1} + \frac{2\nu(T_2^{n+1} - T_1^{n+1} + T_2^n - T_1^n)}{\Delta z_1(\Delta z_1 + \Delta z_2)} \right], \\ T_k^{n+1} &= T_k^n + \frac{\Delta t}{2} \left[-\frac{\nu(T_k^{n+1} - T_{k-1}^{n+1} + T_k^n - T_{k-1}^n)}{\Delta z_k(\Delta z_k + \Delta z_{k-1})} + \frac{\nu(T_{k+1}^{n+1} - T_k^{n+1} + T_{k+1}^n - T_k^n)}{\Delta z_k(\Delta z_{k+1} + \Delta z_k)} \right] \quad (k = 2, \dots, N), \end{aligned} \quad (4.5.98)$$

where

$$G_1^{n+1} = G_1^n + \Delta t \left[\frac{\partial G_1}{\partial t} \right]^{n+1/2} = G_1^n + \Delta t \left[\frac{\partial G_1}{\partial T_1} \frac{\partial T_1}{\partial t} \right]^{n+1/2} \cong G_1^n + \left[\frac{\partial G_1}{\partial T_1} \right]^n (T_1^{n+1} - T_1^n).$$

If T_N is given, these elliptic equations can be solved. In MSM, T_4 is fixed by the climatological values during forecast. (See 4.4.8(d.5) about obtaining the climatological values.)

ρ_c and ν are set as to land use and surface kind.

Wetness (efficiency of vaporization from surface) is also predicted by force restore method based on Deardorff (1978).

4.5.10 Parallelization

The automatic parallelization (SMP) by a Fortran compiler and the Message Passing Interface (MPI) are used for the parallelization among threads and processes, respectively. Two-dimensional decomposition (Aranami and Ishida, 2004, Fig. 4.5.5) is adopted. The width of the halo region is set to unity and the values of the halo region are exchanged at necessary time to calculate the lower-order advection and interpolation. Another communication way is used to calculate the higher-order advection. A special node is exclusively spared for the output process to avoid wasting time by the output result on disk (Fig. 4.5.6). As the number of nodes increase, adopting output node saves more computational time. The computational results using arbitrary number of MPI processes exactly coincide with each other.

One MPI process consists of 8 threads and 78 processes (divided into 6 for x direction and 13 for y direction) are used for calculation and 1 process used for output, operationally. The number of nodes used for operational run is 40 and the elapse time of the calculation is about 17 minutes for 15-hour forecast on Hitachi SR11000/K1.

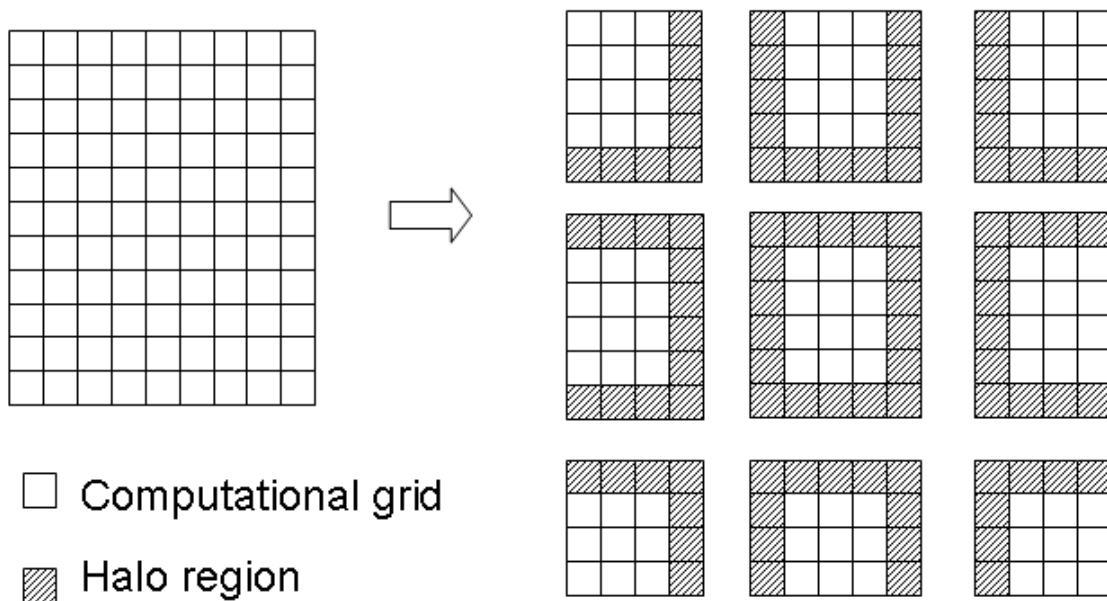


Fig. 4.5.5 The whole computational domain (left) and the domain distributed to MPI processes with halo regions (right).

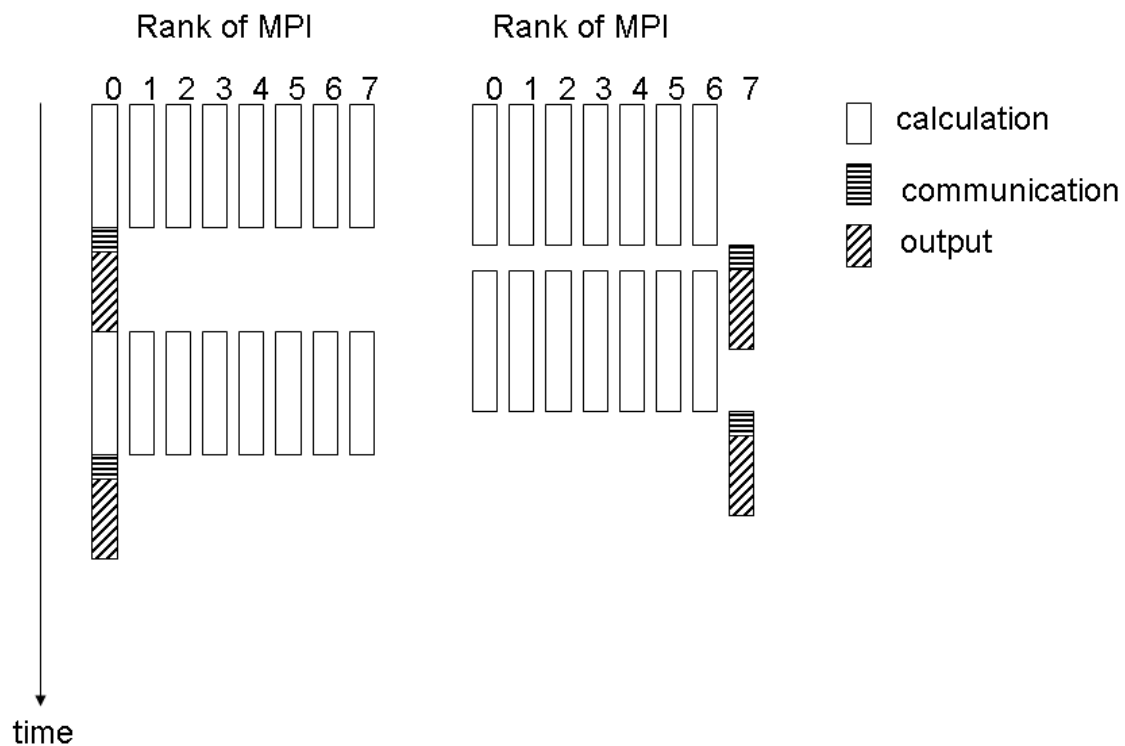


Fig. 4.5.6 A diagram of calculation without output node (left) and with output node (right) using 8nodes.

4.5.11 Forecast Performance

The verification of quantitative precipitation forecast is particularly emphasized to evaluate the performance of MSM. Figure 4.5.7 and Fig. 4.5.8 show the monthly threat and bias scores for 3 hourly precipitation predicted by MSM with the threshold of 10mm (See 4.9). The verification period is from March 2001 to December 2006. The verification grid size is 20km, and the verification is done using “Radar–Raingauge Analyzed Precipitation” (hereafter R-A. See 5.4.1). The horizontal resolution of the R-A was about 2.5km until February 2006, but has been enhanced up to 1km since March 2006. In the winter, the accuracy of the R-A is degraded by loss of radar observable area, so that bias scores have shown tendencies of overestimation of precipitation (Fig. 4.5.8).

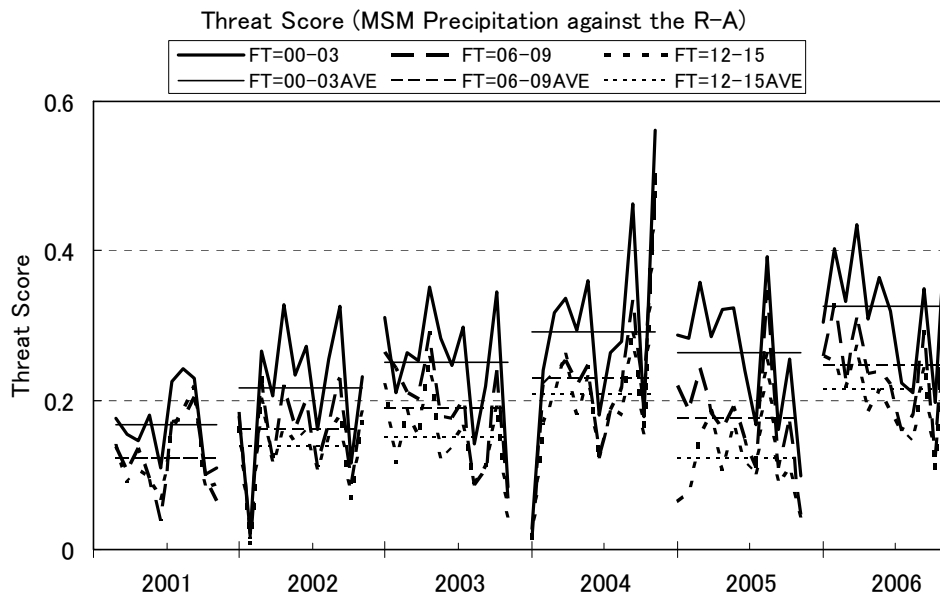


Fig. 4.5.7 The monthly threat scores for 3hourly precipitation by MSM against the R-A with the threshold of 10mm/3h and within 20km verification grid. The verification period is from Mar. 2001 to Dec. 2006. The thin line means annual average. FT means forecast time from initial time.

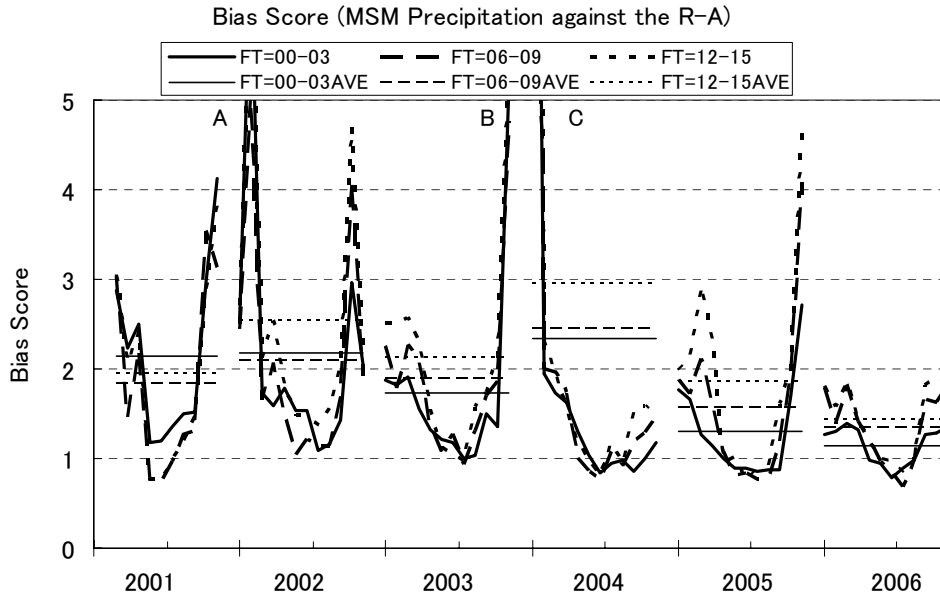


Fig. 4.5.8 Same as Fig. 4.5.7 but bias scores. 'A' means 6.7 (FT=00-03), 5.0 (FT=06-09), and 6.6 (FT=12-15) in Feb. 2002. 'B' means 5.1 (FT=00-03), 4.8 (FT=06-09), and 5.5 (FT=12-15) in Dec. 2003. 'C' means 14.6 (FT=00-03), 15.0 (FT=06-09), and 20.0 (FT=12-15) in Jan. 2004.

References

- Aranami, K. and J. Ishida, 2004: Implementation of two dimensional decomposition for JMA nonhydrostatic model. *CAS/JSC WGENE Res. Activ. Atmos. Oceanic Model.*, **34**, 0301–0302.
- Beljaars, A.C.M. and A.A.M. Holtslag, 1991: Flux parameterization over land surfaces for atmospheric models. *J. Appl. Meteor.*, **30**, 327–341.
- Briegleb, B.P., 1992: Delta-Eddington Approximation for Solar Radiation in the NCAR Community Climate Model. *J. Geophys. Res.*, **97**, 7603–7612.
- Deardorff, J.W., 1978: Efficient prediction of ground surface temperature and moisture, with inclusion of layer vegetation. *J. Geophys. Res.*, **83**, 1889–1903.
- Ebert, E.E. and J.A. Curry, 1992: A parameterization of ice cloud optical properties for climate models. *J. Geophys. Res.*, **97**, 3831–3836.
- Fritsch, J.M. and C.F. Chappell, 1980: Numerical prediction of convectively driven mesoscale pressure systems. Part I: Convective parameterization. *J. Atmos. Sci.*, **37**, 1722–1733.
- Gal-Chen, T. and R.C.J. Somerville, 1975: On the use of a coordinate for the solution of the Navier-Stokes equation. *J. Comp. Phys.*, **17**, 209–228.
- Goldman, A. and T.G. Kyle, 1968: A comparison between statistical model and line calculation with application to the 9.6 μm ozone and the 2.7 μm water vapor bands. *Appl. Opt.*, **7**, 1167–1177.
- Goody, R.M., 1952: A statistical model for water vapor absorption. *Quart. J. Roy. Meteor. Soc.*, **78**, 165–169.
- Hack, J.J., 1998: Sensitivity of the simulated climate to a diagnostic formation for cloud liquid water. *J. Climate*, **11**, 1497–1515.
- Houghton, J.T., 1977: *The physics of atmospheres*. Cambridge Univ. Press. 203pp.
- Ikawa, M. and K. Saito, 1991: Description of a non-hydrostatic model developed at the Forecast Research Department of the MRI. *MRI Tech. Rep.*, **28**, 238 pp.
- Kain, J. S., 2004: The Kain-Fritsch convective parameterization: An update. *J. Appl. Meteor.*, **43**, 170–181.
- Kain, J.S. and J.M. Fritsch, 1990: A one-dimensional entraining/detraining plume model and its application in convective parameterization. *J. Atmos. Sci.*, **47**, 2784–2802.
- Kato, T., 1995: A box Lagrangian rain-drop scheme. *J. Meteor. Soc. Japan*, **73**, 241–245.
- Kato, T., 1998: Numerical simulation of the band-shaped torrential rain observed southern Kyushu, Japan on 1 August 1993. *J. Meteor. Soc. Japan*, **76**, 97–128.
- Kiehl, J.T. and C.S. Zender, 1995: A Prognostic Ice Water Scheme for Anvil Clouds. *World Climate Programme Research, WCRP-90*, WMO/TD-No. 713, 167–188.
- Kitagawa, H., 2000: Radiation scheme. *Report of Numerical Prediction Division*, **46**, 16-31 (in Japanese, Suuchiyohouka Bessatsu Houkoku).
- Klemp, J.B. and R.B. Wilhelmson, 1978: The simulation of three-dimensional convective storm dynamics. *J. Atmos. Sci.*, **35**, 1070–1096.

- Kondo, J., 1975: Air-sea bulk transfer coefficients in diabatic conditions. *Bound. Layer Met.*, **9**, 91–112.
- Lin, Y.-L., R.D. Farley, and H.D. Orville, 1983: Bulk parameterization of the snow field in a cloud model. *J. Climate Appl. Meteor.*, **22**, 1065–1092.
- Louis, J.F., M.Tiedtke, and J.F. Geleyn, 1982: A short history of the operational PBL parameterization at ECMWF. In *Proc. Workshop on Planetary Boundary Layer Parameterization*, 59–79, Reading, United Kingdom, 1982. ECMWF.
- Nakamura, H., 1978: Dynamical effects of mountains on the general circulation of atmosphere: 1. Development of finite-difference schemes suitable for incorporating mountains. *J. Meteor. Soc. Japan*, **56**, 317–397.
- Ohno, H. and M. Isa, 1984: A statistical relation between GMS-viewed cloud amount and relative humidity. *Tenki*, **31**, No.8, 493–495 (in Japanese).
- Ou, S.-C. and K.-N. Liou, 1995: Ice microphysics and climate temperature feedback. *Atmos.Res.*, **35**, 127–138.
- Robert, A.J., 1966: The integration of a low order spectral form of the primitive meteorological equations. *J. Meteor. Soc. Japan*, **44**, 237–245.
- Roberts, R.E., J.A. Selby, and L.M. Bibermann, 1976: Infrared continuum absorption by atmospheric water vapor in the 8–12 μm window. *Appl. Opt.*, **15**, 2085–2090.
- Rodgers, C.D. and C.D. Walshaw, 1966: The computation of infrared cooling rate in planetary atmospheres. *Quart. J. Roy. Meteor. Soc.*, **92**, 67–92.
- Roewe, D. and K.-N. Liou, 1978: Influence of cirrus clouds on the infrared cooling rate in the troposphere and lower stratosphere. *J. Appl. Meteor.*, **17**, 92–106.
- Saito, K., 1997: Semi-implicit fully compressible version of the MRI mesoscale nonhydrostatic model – Forecast experiment of the 6 August 1993 Kagoshima torrential rain. *Geophys. Mag. Ser.*, **2**, 109–137.
- Saito, K., T. Fujita, Y. Yamada, J. Ishida, Y. Kumagai, K. Aranami, S. Ohmori, R. Nagasawa, S. Kumagai, C. Muroi, T. Kato, H. Eito, and Y. Yamazaki, 2006: The Operational JMA Nonhydrostatic Mesoscale Model. *Mon. Wea. Rev.*, **134**, 1266–1298.
- Skamarock, W.C. and J.B. Klemp, 1992: The stability of time split numerical methods for the hydrostatic and nonhydrostatic elastic equation. *Mon. Wea. Rev.*, **120**, 2109–2127.
- Slingo, J., 1989: A GCM parameterization for the short wave radiative properties of water cloud. *J. Atmos. Sci.*, **46**, 1419–1427.
- Sugi, M., K. Kuma, K. Tada, K. Tamiya, N. Hasegawa, T. Iwasaki, S. Yamada, and T. Kitade, 1990: Description and performance of the JMA operational global spectral model (JMA–GSM88). *Geophys. Mag.*, **43**, 105–130.
- Sun, W.Y. and C.Z. Chang, 1986: Diffusion model for a convective layer. Part I: Numerical simulation of convective boundary layer. *J. Climate Appl. Meteor.*, **25**, 1445–1453.